Paragliders' Launch Trajectory is Universal

Quentin da Cruz Lopes, Sophie Ramananarivo, Caroline Cohen, Michael Benzaquen

Paragliders' Launch Trajectory is Universal

Quentin Da Cruz Lopes,[1] Sophie Ramananarivo,[1] Caroline Cohen,[1] and Michael Benzaquen[1,*]
[1] *LadHyX UMR CNRS 7646, École polytechnique, 91128 Palaiseau Cedex, France*

(Dated: May 18, 2022)

We design, build and run a reduced-scale model experiment to study the paragliding inflation and launching phase at given traction force. We show that the launch trajectory of the glider is universal, that is, independent of the strength of the exerted force. As a consequence, the length of the take-off run required for the glider to reach its "ready to launch" vertical position is also universal. We successfully confront our results to real scale experiments, and show that such universality can be understood through a simple theoretical model.

INTRODUCTION

Paragliding is a young adventure sport (dating back to early 80's) consisting in flying lightweight, free-flying, foot-launched glider aircrafts with no rigid primary structure [8, 11]. For a physicist, it truly is a bottomless drawer of fascinating unexplored phenomena, combining a variety of fields covering fluid mechanics, fluid-structure interactions, flight mechanics, materials science, micrometeorology, and even game theory in the context of understanding exploration-exploitation optima in paragliding competitions.

Since the first prototypes, paraglider wings haven't ceased to evolve, both in terms of performance and security. While most of the research done by paragliding manufacturers (see e.g. [2, 6]) has focused on optimising wings for steady flight phases, unsteady regimes have only received limited attention [10]. In particular, many questions remain unsolved when it comes to the dynamics of stalls or wing collapses combined with the aircraft specific pendulum-motion. Further independent and fundamental research is susceptible to provide quantitative elements for improving the safety of modern gliders, the approval of which is now based on the rather qualitative feeling of test pilots. In addition, accidentology studies shows that a substantial fraction of accidents occur at take-off [7, 13], which makes crucial the study of the launching phase.

In the present communication, we investigate the dynamics of the launching phase: How does a seemingly simple rag inflate when pulled by the pilot to become a rather stable aircraft in just a matter of seconds? We design, built and run a reduced-scale model experiment to study the paragliding inflation and launching phase at given traction forces. We find that the launch trajectory is universal – in the sense that it does not depend on the strength of the exerted force – and as a result so is the distance required for the glider to reach its "ready to launch" vertical position. Due to the potential limitations of the model experiment, namely the difficulty to scale down the stiffness of the materials (fabric and lines), we decided to perform real scale experiments on the field which nevertheless showed excellent agreement with the reduced scale results.

I. REDUCED-SCALE EXPERIMENT

With the aim of working in a controlled environment to ensure reproducibility of our results, we start with a reduced-scale experiment in which a small paraglider is pulled from its risers along a horizontal 3 m long guide rail by a wire and pulley system (see Fig. 1). To mini-

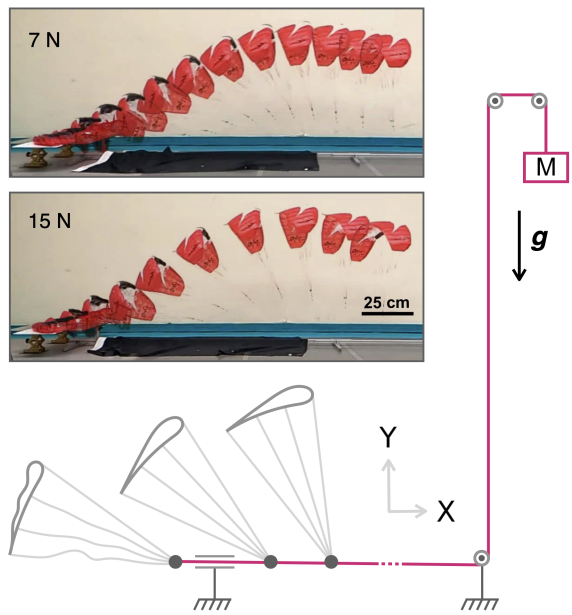

Figure 1: Reduced-scale experiment (see Sec. I). The top left captions show chronophotographic runs of the experiment with respectively $Mg = 7.0\,\mathrm{N}$ and $15.0\,\mathrm{N}$. The timestep between shots is 40 ms.

* michael.benzaquen@polytechnique.edu

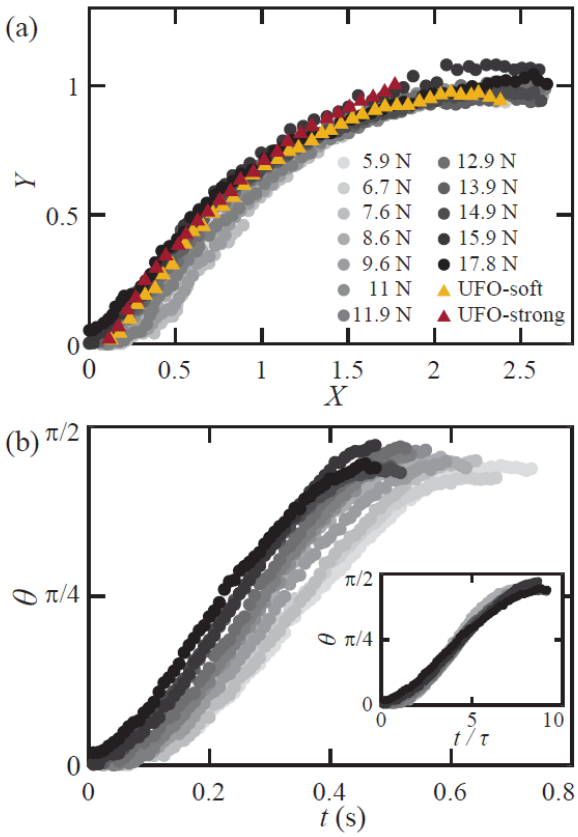

Figure 2: (a) Dimensionless trajectory of the trailing edge of a reduced-scale glider during launching at constant traction force with $X = x/\ell$ and $Y = y/\ell$, for different values of the traction force (denoted by the grayscale, bullet markers). Corresponding trajectories for a real-scale AirDesign® UFO glider (triangle markers). (b) Time evolution of the glider's angle θ. Rescaling with the characteristic timescale $\tau = \sqrt{m\ell/F_O}$ collapses the data (inset).

mize friction, the paraglider is fastened to a ring looped around a taught string that serves as the guide.

Consistent with realistic conditions, we chose to work with given traction force rather than given velocity. Indeed, when a pilot launches he exerts a given physical effort. While such effort is most certainly not perfectly constant over the launching phase, assuming constant force is a good approximation. It is indeed what the pilot attempts to achieve. Here, the constant force is ensured via a falling mass M attached to the wire and pulley system.

During the launching process, one would like to distinguish two phases: (i) that during which the chambers fill with air to give the aircraft its wing shape ensuring lift, and (ii) the phase where the "inflated" wing rises from the horizontal to the vertical position. Yet, these two phase are not separable in time as they take place somewhat simultaneously, at least in the early stages. Here we use a 130 cm flat wingspan single-surface glider (Oxy 0.5 model designed by *Opale Paramodels*), see Tab. I. This is convenient because for single-surface gliders, the time overlap between phases (i) and (ii) appears to be much weaker, due to the very rapid dynamics of phase (i). In the top left panels of Fig. 1 one can see that the glider is fully inflated when the trailing edge (used to track its position and to identify $t = 0$ in the following) leaves the ground. See Sec. IV for a discussion on regular double-surface gliders.

Figure 2a displays the dimensionless trajectory $Y(X)$ of the trailing edge during launching runs with different values of the traction force, ranging from 5.9 to 17.8 N. Its position is tracked manually using ImageJ for image analysis. Note that the taught string that is used as a guide rail tends to distort a little under the pulling action of the glider. To account for this upwards shift, we substract the height of the attachment point to that of the trailing edge. Strikingly enough all the trajectories fall on top of each other in Fig. 2a, thereby indicating the independence to the traction force and universality of the launch trajectory. The traction force however determines the speed at which the paraglider moves along this universal trajectory, as shown in the time-evolution of its angle $\theta(t)$ in Fig. 2b. As shall be discussed in Section III, this force F_O sets the characteristic time scale of the ascent $\tau = \sqrt{m\ell/F_O}$, with m the wing mass and ℓ the length of the glider lines (see the collapse of data recasted as a function of t/τ in the inset of Fig. 2b).

Glider	Oxy 0.5	UFO 13
Flat wingspan (m)	1.3	8.04
Flat area (m^2)	0.5	13.0
Aspect ratio	4.2	4.9
Cells	17	27
Weight (kg)	0.05	1.36
Takeoff weight (kg)	–0.3	45–80

Table I: Glider characteristics for the Oxy 0.5 wing (*Opale Paramodels*) and the UFO 13 (*AirDesign Gliders*). For the detailed line charts see manufacturer's websites [3, 4].

II. REAL SCALE EXPERIMENT

Concerned with the difficulty to downscale all characteristics of a real glider (as mentioned above), we decided to confront our results to real scale experiments (see Fig. 3). Using a 13 m^2 flat single-surface glider (AirDesign® gliders UFO wing), see Tab. I, we were able to record a few launches on a calm day at Puy de Dome (Auvergne, France). A seasoned test pilot was

Figure 3: Real scale experiment (see Sec. II). The timestep between shots is 200 ms.

asked to launch with low and strong traction strength respectively. Unlike laboratory experiments, a slight wind was present here, with speeds around 7 m.s^{-1} measured during each run. To account for this and be able to compare both configurations, the wind is treated as an additional forward motion of the paraglider at constant speed in a still air environment. As one can see in Fig. 2a the trajectories collapse with their reduced-scale counterparts, thereby validating the reduced-scale methodology.

III. THEORETICAL MODEL

In this section we present a simple theoretical model to account for the experimental results (see Fig. 4). We assume that a rigid glider of mass m is characterised by its lift and drag coefficients [9, 12], commonly denoted $C_L(\alpha)$ and $C_D(\alpha)$ respectively, where α is the angle of attack. The lift and drag forces applying to the center of pressure M (or aerodynamic center) write:

$$\boldsymbol{L} = \tfrac{1}{2}\rho S C_L(\alpha) \boldsymbol{V}_M^2 \boldsymbol{e}_\perp \quad (1a)$$

$$\boldsymbol{D} = \tfrac{1}{2}\rho S C_D(\alpha) \boldsymbol{V}_M^2 \boldsymbol{e}_\parallel, \quad (1b)$$

with ρ the air density, S the planform (projected) wing area, and V_M the norm of the velocity of M in the lab's frame of reference (or true airspeed). We further assume that the center of pressure is attached to the traction point O with a rigid weightless line of length ℓ exerting a tension $\pm\boldsymbol{T}_e = \mp T_e \boldsymbol{e}_r$ on both its extremities. Finally, the traction point is constrained to move along the x axis only, and submitted to a horizontal force $F_O = F_O \boldsymbol{e}_x$.

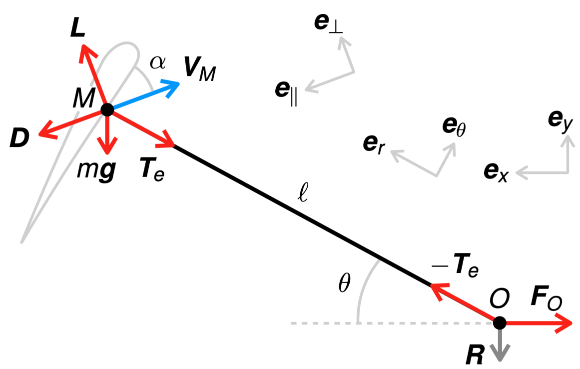

Figure 4: Schematics supporting the theoretical model (see Sec. III).

Applying Newton's second law to point M, together with the angular momentum theorem relative to O yields the following dimensionless equations (see Appendix):

$$\dot{V}_O \cos\theta - \dot{\theta}^2 + \tfrac{1}{\cos\theta} = \tfrac{1}{2}\rho S V_M^2 (C_L \cos\alpha + C_D \sin\alpha) \quad (2)$$

$$\ddot{\theta} + \tfrac{\tan\theta}{\cos\theta} - \dot{\theta}^2 \tan\theta = \tfrac{1}{2}\rho S V_M^2 \big(C_L[\sin\alpha + \cos\alpha\tan\theta] + C_D[\sin\alpha\tan\theta - \cos\alpha]\big), \quad (3)$$

with dimensionless variables $t \to t/\tau$, $V \to V\tau/\ell$ with $\tau^2 = m\ell/F_O$, $\rho \to \rho\ell^3/m$ and $S \to S/\ell^2$, and where we have neglected gravity forces. As one can see, F_O only appears in the equations through the timescale τ used to non-dimensionalize time, thereby explaining the universality of the trajectories observed in Sections I and II. For the small-scale glider, one has $\tau \approx 0.3/\sqrt{F_O}$ s, while for the real scale UFO wing $\tau \approx 3/\sqrt{F_O}$ s. This typical timescale allows to compute the typical force that is required to launch in a given amount of time.

Equations (2) and (3) constitute a system of two coupled ordinary differential equations, with only θ, V_O and their derivatives as unknowns (see Appendix). Therewith, they can be jointly solved numerically for given C_L, C_D. We do not expect standard forms of C_L, C_D (see e.g. [1]) to provide good quantitative agreement with the experiments for the following reason. Typical lift and drag coefficients are only valid in stationary conditions. As such, they are not expected to stand in the fundamentally unsteady conditions of the launching phase (for one thing, within steady flight theory the wing should stall in the very beginning of the launch as the angle of incidence $\alpha \to \pi/2$, which is obviously not the case here). Measuring unsteady lift and drag coefficients would be very interesting, but doing so comes with its own difficulties and would require an entire and independent analysis, way beyond the scope of the present story. Note that such unsteady lift and drag coefficients are expected to be highly intricate as in the early stages the wing is not fully inflated, and thus its very shape varies over time (this might explain why the wing doesn't stall in the early stages). Our main claim here is thus on the universality and the identification of the timescale τ, not on the precise theoretical trajectory, which is left for future research.

IV. DISCUSSION

This study revealed a number of other exciting questions, such as the optimal folding of the wing for a comfortable launch in strong wind conditions, or the differences between regular and single skin wings during unsteady phases, and the launching phase in particular. Single-surface gliders are known to launch much faster than their regular counterparts. This is often attributed to the fact that they are lighter and thus have less inertial effects, but we believe it can also be related to the fact that the inflation phase is much faster, as argued in Section I. For regular double skin gliders the question of the simultaneity for the chambers air-filling and rising phases, is an intricate one. Indeed, one expects that the lift coefficient grows progressively as the chambers fill with air, which explains why the wing starts to take off before the glider is fully inflated. To quantitatively unravel the role of these phases, one could think of combining high speed camera filming of a static inflation experiment (in which the glider is attached to the ground at its trailing edge), together with an experiment on rigid wings (printed in 3D or cut with a hot wire in polystyrene), and compute the characteristic times of each isolated phase to disentangle their interactions. One should bare in mind that while seemingly irrelevant in the present communication, the limitations to scale down the stiffness of the materials in our experiments might have important implications on the characteristics of the inflation phase. These ideas are left for future research.

ACKNOWLEDGEMENTS

We deeply thank Alexandre Darmon for agreeing to serve as test pilot during the real scale experiments and for proofreading the manuscript, as well as Henri Montel (Freedom Parapente at Puy de Dôme) for lending the gliders and several discussions.

[1] Sarah Becker. Experimental study of paraglider aerodynamics. *Yüksek Lisans, Imperial College London, Department of Aeronautics, Endüstri Mühendisliği Bölümü, London*, 2017.

[2] Diego Muniz Benedetti. *Paragliders flight dynamics.* Universidade Federal de Minas Gerais, 2012.

[3] AD UFO Brochure. Airdesign gliders, 2022.

[4] Oxy 0.5 Brochure. Opale paramodels, 2022.

[5] John Charles Butcher. *Numerical methods for ordinary differential equations.* John Wiley & Sons, 2016.

[6] Rene Falquier. *Longitudinal Flight Mechanics of Paraglider Systems.* 2019.

[7] Gunter Fasching, Gerhard Schippinger, and Rudolf Pretscher. Paragliding accidents in remote areas. *Wilderness & Environmental Medicine*, 8(3):129–133, 1997.

[8] Mr Nicholas Landell-Mills. Paragliding explained by newtonian physics. 2022.

[9] Joan Marc Moreno Colilles. Aerodynamic performance of a paraglider wing. B.S. thesis, Universitat Politècnica de Catalunya, 2017.

[10] Marcel Müller, Abid Ali, and Alfred Tareilus. Modelling and simulation of a paraglider flight. In *Proc. 9th EUROSIM Congress on Modelling and Simulation*, number 142, 2018.

[11] Menegoz Pierre-Paul and Jacques Alain. Le manuel du vol libre delta parapente. *Fédération Française du Vol Libre*, 2005, édition 2020.

[12] J Ross. Computational aerodynamics in the design and analysis of ram-air inflated wings. In *12th AIAA Aerodynamic decelerator Systems Technology Conference*, pages 10–13, 1993.

[13] Robin Soleil. *Accidentologie du parapente chez les compétiteurs.* 2016.

APPENDIX

Consider Fig. 4. The angular momentum of the glider relative to O reads $m\ell^2\dot{\theta}\boldsymbol{e}_z$. The forces acting on M in the non-inertial frame of reference attached to O are the lift and drag forces, as given by Eqs. (1a) and (1b), the weight $m\boldsymbol{g}$, the tension $-T_e\boldsymbol{e}_r$, and the fictitious force $-m\dot{V}_O\boldsymbol{e}_x$, where V_O denotes the velocity of point O in the inertial frame of reference. The angular momentum theorem then writes:

$$m\ell\ddot{\theta} = L\sin\alpha - D\cos\alpha - mg\cos\theta + m\dot{V}_O\sin\theta, \tag{4}$$

where the right hand side denotes the torque on M with respect to O along $\boldsymbol{e}_z$. Newton's second law to point M along $\boldsymbol{e}_r$ writes:

$$-m\ell\dot{\theta}^2 = L\cos\alpha + D\sin\alpha - mg\sin\theta - T_e - m\dot{V}_O\cos\theta. \tag{5}$$

The angle of attack α and the true airspeed V_M are kinematically related to θ through:

$$\cos\alpha = \frac{\ell\dot{\theta} - V_O\sin\theta}{\sqrt{V_O^2\cos^2\theta + (\ell\dot{\theta} - V_O\sin\theta)^2}}; \quad \sin\alpha = -\frac{V_O\cos\theta}{\sqrt{V_O^2\cos^2\theta + (\ell\dot{\theta} - V_O\sin\theta)^2}}; \tag{6}$$

$$V_M^2 = V_O^2\cos^2\theta + (\ell\dot{\theta} - V_O\sin\theta)^2. \tag{7}$$

Finally, applying Newton's second law to massless point O yields:

$$T_e = \frac{F_O}{\cos\theta}, \tag{8}$$

which can be injected into Eq. (5) to eliminate T_e. Therewith, Eqs. (4) and (5) – combined with Eqs. (1a), (1b), (6), (7) and (8) – constitute a system of two coupled ordinary differential equations, with only θ, V_O and their derivatives as unknowns. Isolating $\dot{V}_0$ in (5) and injecting it into (4) finally yields:

$$\dot{\tilde{V}}_O\cos\theta = \dot{\tilde{\theta}}^2 + \frac{1}{2}\tilde{\rho}\tilde{S}\tilde{V}_M^2(C_L(\alpha)\cos\alpha + C_D(\alpha)\sin\alpha) - \tilde{g}\sin\theta - \frac{1}{\cos\theta} \tag{9}$$

$$\begin{aligned}\ddot{\tilde{\theta}} + \frac{\tan\theta}{\cos\theta} - \dot{\tilde{\theta}}^2\tan\theta = {} & \frac{1}{2}\tilde{\rho}\tilde{S}\tilde{V}_M^2[C_L(\alpha)(\sin\alpha + \cos\alpha\tan\theta) + C_D(\alpha)(\sin\alpha\tan\theta - \cos\alpha)] \\ & -\tilde{g}(\cos\theta + \sin\theta\tan\theta)\end{aligned} \tag{10}$$

where we have introduced the dimensionless variables $\tilde{t} = t/\tau$, $\tilde{V} = V\tau/\ell$, $\dot{\tilde{\theta}} = \dot{\theta}\tau$, $\ddot{\tilde{\theta}} = \ddot{\theta}\tau^2$, $\tilde{g} = g\tau^2/\ell$ with $\tau^2 = m\ell/F_O$, $\tilde{\rho} = \rho\ell^3/m$ and $\tilde{S} = S/\ell^2$. Equations (9) and (10) are equivalent to Eqs. (2) and (3) in the main text, where all the $\sim$ have been dropped, and where the gravity terms have been set to zero, given that their contribution turns out to be negligible. If one wishes to solve numerically the equations, this can be done using a standard RK45 method (explicit Runge-Kutta [5]) choosing e.g. $C_L = \mu_L\sin 2\alpha$ and $C_D = \mu_D\sin^2\alpha + cst$ (see [1]). Again, we do not expect quantitative agreement with the experimental trajectories for the reasons presented in Sec. III. The theory is only intended to account for the universality, and the identification of the typical timescale τ.